

The completely renewed and upgraded neutron reflectometer at the TU Delft Reactor Institute

Bannenberg, Lars J.; Bresser, Raymon; van der Ende, Piet; van Exter, Martin; van Goozen, William; Naastepad, Fred; Thijs, Michel A.; Verleg, Malte N.; de Vroege, Kees; Waaijer, Rien

DOI

[10.1063/5.0155888](https://doi.org/10.1063/5.0155888)

Publication date

2023

Document Version

Final published version

Published in

Review of Scientific Instruments

Citation (APA)

Bannenberg, L. J., Bresser, R., van der Ende, P., van Exter, M., van Goozen, W., Naastepad, F., Thijs, M. A., Verleg, M. N., de Vroege, K., Waaijer, R., & van Well, A. A. (2023). The completely renewed and upgraded neutron reflectometer at the TU Delft Reactor Institute. *Review of Scientific Instruments*, 94(11), Article 113901. <https://doi.org/10.1063/5.0155888>

Important note

To cite this publication, please use the final published version (if applicable). Please check the document version above.

Copyright

Other than for strictly personal use, it is not permitted to download, forward or distribute the text or part of it, without the consent of the author(s) and/or copyright holder(s), unless the work is under an open content license such as Creative Commons.

Takedown policy

Please contact us and provide details if you believe this document breaches copyrights. We will remove access to the work immediately and investigate your claim.

RESEARCH ARTICLE | NOVEMBER 08 2023

The completely renewed and upgraded neutron reflectometer at the TU Delft Reactor Institute

Lars J. Bannenberg ; Raymon Bresser ; Piet van der Ende; Martin van Exter ; William van Goozen; Fred Naastepad; Michel A. Thijs ; Malte N. Verleg; Kees de Vroege ; Rien Waaijer; Ad A. van Well 

 Check for updates

Rev. Sci. Instrum. 94, 113901 (2023)

<https://doi.org/10.1063/5.0155888>



View
Online



Export
Citation

CrossMark



www.ssi-instrument.com

PXI module Lock-in Amplifier

Multi-channel Lock-in Amplifier

Up to 8 demodulators

Toolset: Scope, FFT, PID, Sweeper

Customize your own Lock-in Amplifier

DC to 300MHz frequency



The completely renewed and upgraded neutron reflectometer at the TU Delft Reactor Institute

Cite as: *Rev. Sci. Instrum.* **94**, 113901 (2023); doi: [10.1063/5.0155888](https://doi.org/10.1063/5.0155888)

Submitted: 24 April 2023 • Accepted: 17 October 2023 •

Published Online: 8 November 2023



View Online



Export Citation



CrossMark

Lars J. Bannenberg,^{a)} Raymon Bresser, Piet van der Ende, Martin van Exter, William van Goozen, Fred Naastepad, Michel A. Thijs, Malte N. Verleg, Kees de Vroege, Rien Waaijer, and Ad A. van Well

AFFILIATIONS

Faculty of Applied Sciences, Delft University of Technology, Mekelweg 15 2629JB Delft, The Netherlands

^{a)} Author to whom correspondence should be addressed: l.j.bannenberg@tudelft.nl

ABSTRACT

The horizontal time-of-flight neutron reflectometer at the reactor of the Delft University of Technology, The Netherlands, has been completely renewed, relocated, and upgraded and allows for the study of air/liquid, solid/liquid, and solid/air interfaces. Innovations in the redesign include (i) a completely flexible double disk chopper system allowing to choose the optimal wavelength resolution with exchangeable neutron guide sections between the chopper disks to increase intensity, (ii) a movable second diaphragm just before the sample position to better control the beam footprint on the sample and effectively decrease counting times, and (iii) guides along the entire flight path of the neutron reflectometer. The performance of the renewed reflectometer is illustrated with measurements of hydrogen sensing materials.

© 2023 Author(s). All article content, except where otherwise noted, is licensed under a Creative Commons Attribution (CC BY) license (<http://creativecommons.org/licenses/by/4.0/>). <https://doi.org/10.1063/5.0155888>

I. INTRODUCTION

Neutron reflectometry is a technique that can be used to obtain information about the thickness, composition, and roughness of thin films and other layered structures with layer thicknesses from a few to over hundreds of nanometers. Analogous to x-ray reflectometry, it measures the fraction of neutrons (photons) that are reflected by flat surfaces and interfaces as a function of the momentum transfer $Q = 4\pi \sin \theta / \lambda$ with λ being the neutron's wavelength and θ being the glancing angle, i.e., the angle between the incident neutron beam and the surface. These reflection data are subsequently modeled to obtain a scattering length density profile, on the basis of which the composition, thickness, and roughness of each of the sample's layers can be determined. Neutron reflectometry can be used to non-destructively study both liquid and solid samples under a variety of different experimental conditions and finds a wide range of applications in the study of surfaces and interfaces of thin films, multilayers and coatings in soft matter, materials science, and hard matter. Examples include surfactants, polymers, membranes for biology and fuel cells, protein adsorption, and electrochemistry, e.g., battery material and corrosion studies, photovoltaic systems, and hydrogen storage and sensing materials.

For over 30 years, neutron reflectometers have existed at research reactors and neutron spallation sources. Neutron reflectometers can be divided into two major designs: monochromatic

and time-of-flight (TOF) reflectometers. In a monochromatic neutron reflectometer, the wavelength is fixed and the incoming angle is changed to vary Q , while in TOF, a pulsed neutron beam with a wide range of neutron wavelength ("white neutron beam") is used. The wavelength is determined by measuring the flight time from the pulsed source or chopper to the detector for each neutron. Using the known flight distance of the neutron, this is converted in a velocity and subsequently to the neutron wavelength. While at pulsed neutron sources, such as spallation sources, TOF reflectometers are the natural choice, whereas at research reactors, one has the flexibility to be able to use both designs. Then, a pulsed beam is created using a chopper system. TOF reflectometers have the distinct advantage that the balance between flux and resolution can be optimized for each individual sample under investigation, as well as for providing more flexibility in kinetic studies. For this reason, several TOF reflectometers have been constructed worldwide,¹⁻⁷ including the previous version of the ROG neutron reflectometer at the 2.3 MW open pool HOR (Dutch abbreviation for Higher Education Reactor) of the Delft University of Technology, The Netherlands, in the early 1990s.⁸ This reflectometer was previously located inside the reactor hall. In anticipation of the installation of the cold source at the Delft reactor (not installed at the time of writing), a new version of the ROG reflectometer has been constructed inside the guide hall that has a much lower background.

The purpose of this paper is to describe the reconstructed version of the ROG that is capable of studying solid samples and solid/liquid and air/liquid interfaces. Given the relatively low power of the Delft Research Reactor of 2.3 MW [i.e., about ten times lower than that of the FRMII reactor in Munich, Germany; the NIST reactor at Gaithersburg, Maryland, United States of America; and the OPAL reactor near Sydney, Australia, and more than 25 times lower than that of the ILL and high-flux-isotope reactor (HFIR) reactors in Grenoble, France, and Oak Ridge, Tennessee, United States of America, respectively], the focus is on using the neutrons available

in the most efficient way for each experiment to maximize the neutron flux at the sample position, for the desired Q -resolution, and thereby minimizing the counting times. As such, the redesigned ROG features a new flexible chopper in which the inter-disk distance can be continuously varied to allow an optimal intensity–resolution trade-off, while various guide segments can be inserted within minutes to maximize the flux. Furthermore, a computer controlled and movable diaphragm, also referred to as a slit, has been installed in front of the sample. This allows positioning the diaphragm as close as possible to the sample, allowing better control of the foot-

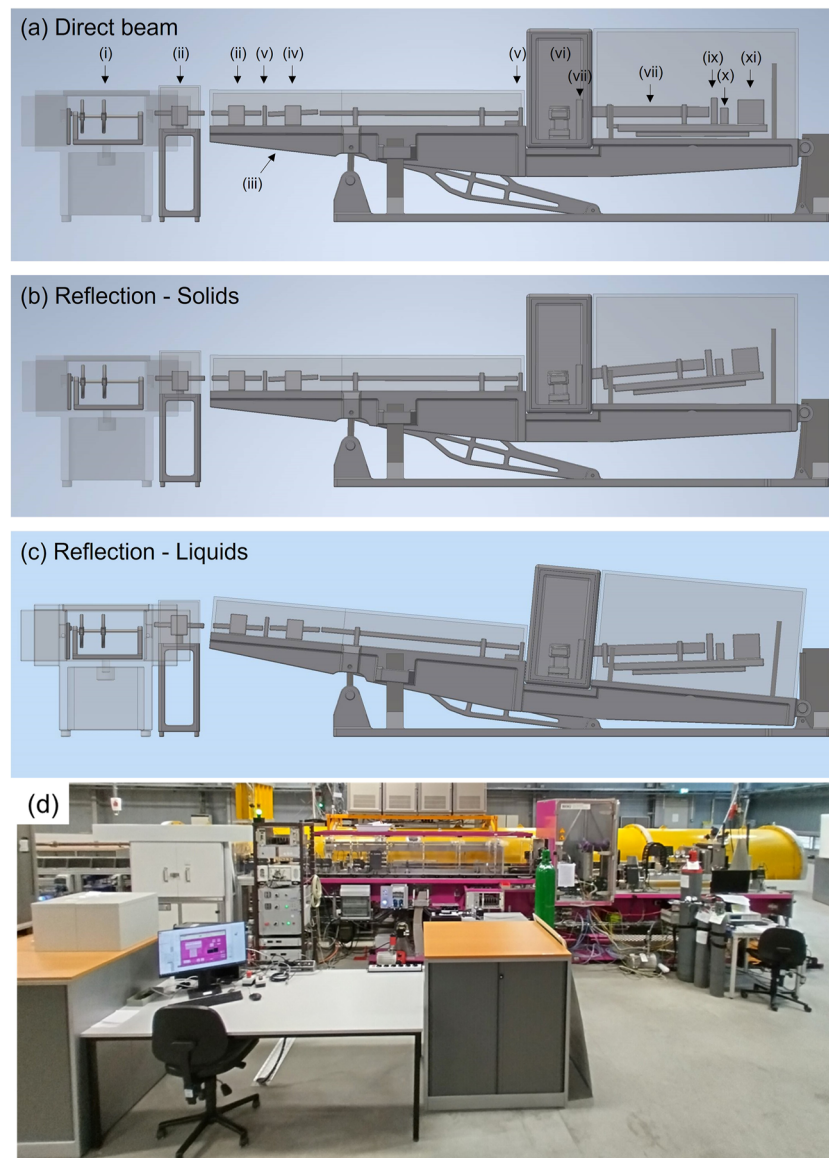


FIG. 1. Schematic of the ROG in (a) direct beam configuration, (b) the configuration for measuring the reflectivity of solids (frame and incoming flight path horizontal and sample and detector tilted), and (c) the configuration for measuring the reflectivity of liquids (frame and incoming flight path tilted and sample horizontal and detector tilted). The components indicated with roman numerals are explained in the text. (d) Photograph of the ROG neutron reflectometer.

print on the sample (i.e., the penumbra is minimized). Therefore, to achieve the same resolution, a larger diaphragm opening can be selected, yielding a higher intensity and thus shorter counting times. Third, we have installed neutron guides along the entire flight path. Finally, we have made it possible to install a neutron prism after the sample position, allowing for much higher intensity white beam measurements. Rather than using a chopper, which results in a considerable intensity loss, the wavelength is determined by using the wavelength-dependent refractive index of neutrons of the prism to guide different wavelengths to different positions on the position-sensitive detector (RAINBOWS method),^{9–12} of which the results will be discussed in an upcoming manuscript.

II. OVERALL DESIGN AND SPECIFICATIONS

Figure 1 provides a schematic representation of the ROG neutron reflectometer in (a) the configuration with a straight beam path and the configuration for the study of (b) solid samples and solid/liquid interfaces and (c) liquid/air interfaces, as well as a photograph in panel (d). The main difference between these configurations is that in the configuration of Fig. 1(b), the beam path before the sample is completely horizontal and the sample is positioned at an angle with respect to the horizontal, whereas in the configuration of Fig. 1(c) dedicated to liquid–air interfaces, the sample is horizontal and both the incoming and reflected beam are tilted with respect to the horizontal.

The ROG neutron reflectometer is connected to a 19.4 m-long, 40 mm-wide neutron guide, which is connected to the beam tube

R2c ($m = 2$, with 0.5 mm aluminum windows, Swiss Neutronics, Klingnau, Switzerland).^{13,14} In the near future, a cold neutron source will be installed at the entrance of this beam tube. From left to right, the major components of the reflectometer are the (i) chopper located inside the chopper house to create a pulsed neutron beam, (ii) supermirror 1 and supermirror 2 to deflect the neutron beam from the horizontal for liquid/air measurements, (iii) frame that supports and can tilt to allow a sample to be positioned horizontally for liquid/air measurements, (iv) frame-overlap mirror that ensures that slow neutrons with long-wavelengths from the neutron pulse are filtered such that they are not accidentally detected in the next time-of-flight frame with an erroneously determined wavelength, (v) diaphragm 1 and diaphragm 2 to control the angular resolution and the footprint on the sample, (vi) sample compartment with a sample table of which the height and angle can be controlled, (vii) diaphragm 3 to block the direct beam and minimize the background, (viii) detector table of which the angle can be adjusted and on which a neutron prism can be mounted, (ix) diaphragm 4 to minimize the background on the detector, (x) the ^3He tube detector, and (xi) Position Sensitive Detector (PSD) and beam stop. Between all components, evacuated neutron guides are positioned to prevent intensity losses due to the horizontal beam divergence, thereby maximizing the flux by minimizing absorption and background originating from the air scatter of neutrons. Together, these components ensure the possibilities listed in Table I.

Motion control is performed using DC powered servo motors or stepper motors in combination with absolute encoders. These motors operate at either 40 or 24 V and are powered by two power supplies (Delta Elektronika, Zierikzee, The Netherlands). The

TABLE I. Specifications of the ROG neutron reflectometer.

Chopper and resolution	Double-disk chopper with variable inter-disk-distance (0.18–0.68 m) with a maximum frequency distance of 25 Hz. Typical operation with an inter-disk of 0.3 m results in $\Delta\lambda/\lambda \approx 0.025$ and $\Delta Q/Q \approx 0.04$
Beam width at the sample position	40 mm
Sample table	± 75 mrad, ± 5 mm vertical displacement, maximum carrying weight of 150 kg
Wavelength range	$0.12 < \lambda < 1.2$ nm (thermal spectrum)
Detectors	^3He detector and a 100 mm-high 1D position sensitive detector (PSD) with 512 pixels and 0.3 mm resolution (Sec. III F)
Sample-to-detector distance	2.065 m for ^3He detector and 2.154 m for PSD
Chopper-to-sample distance	~ 5.5 m (see Ch 4)
Time-of-flight distance	~ 7.5 m (see Ch 4)
Incident angle	Solids: $-25 < \theta < 75$ mrad Liquids: $0 < \theta < 75$ mrad
Wavevector transfer	Solids: $0 < Q < 3 \text{ nm}^{-1}$ liquids: $0 < Q < 3 \text{ nm}^{-1}$

motion control is performed using Eltrex Motion BV, Breda, The Netherlands. A National Instruments PXI 1042Q real time system equipped with a PXI-8512 High-Speed/Flexible Data (FD) Controller Area Network (CAN) Interface is used for communication. A PXI 7841R FPGA is used for the detector (National Instruments, Austin, Texas, USA).

III. COMPONENTS

A. Double-disk chopper

1. Construction

To facilitate an optimal balance between resolution and intensity, a double-disk chopper with variable inter-disk spacing has been constructed^{15,16} (Fig. 2). The chopper itself consists of an 802.5 mm long non-magnetic stainless steel chopper axis with a cross section that has a Polygon P4C PW30.25 profile (Stemin Breitbach, Lochem, The Netherlands). The axis is supported at three positions to ensure a well-balanced and rigid system, and a length scale is indicated on the chopper axis.

Two identical disks are mounted on the chopper axis with a radius of $R = 205$ mm, an opening of $\phi = 20^\circ$ and $N = 2$ slots per disk. The disks have phase difference $\varphi = 20^\circ$ with respect to each other. These disks are made of 4 mm thick boron nitride and ~ 2 mm thick boron rubber sandwiched between two disks of aluminum and have a total thickness of 11 mm [Fig. 2(b)]. The first of these two disks has a fixed position on the chopper axis, while the second one can be moved along the chopper axis to achieve an inter-disk distance of $z_0 = 180$ –680 mm. A small hole inside the first chopper disk is used in combination with a light source and detector to generate a trigger signal for the software. The axis can be used with a chopper frequency of $0 < f < 20$ Hz. The axis is powered using a Tetra TC60 1.3 21 370 W servo motor (Motor Power Company, Castelnovo Sotto, Italy) and connected to the gearwheel by a toothed belt. The number of teeth of the gearwheel on the motor and on the chopper axis is different to avoid resonances. The motor control was made using Eltrex Motion BV, Breda, The Netherlands, and chopper balancing was performed using Elma BV, Soesterberg, The Netherlands, leading to a maximum horizontal displacement velocity of 0.53 mm s⁻¹.

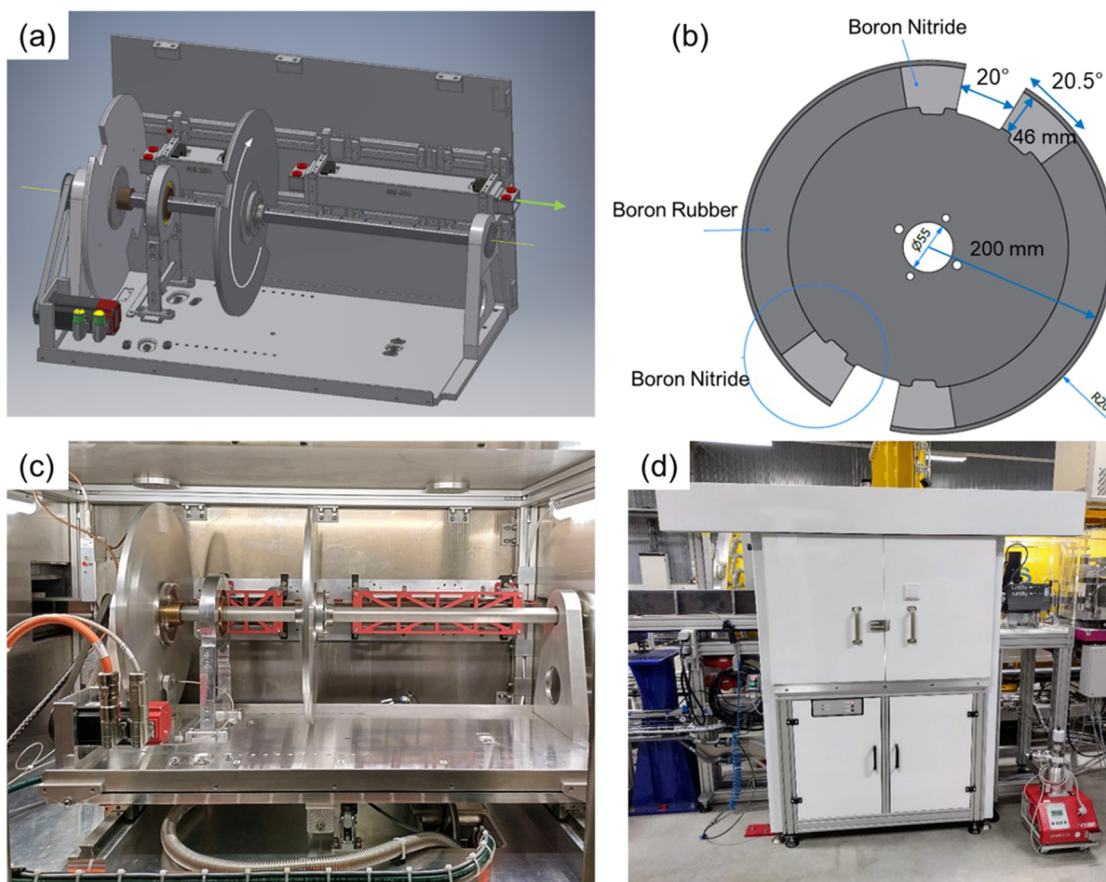


FIG. 2. Double-disk chopper system. (a) 3D view of the double disk chopper with an inter-disk distance of 300 mm. The neutrons pass from left to right. (b) Detailed drawing of one chopper disk. (c) Photograph of the double-disk chopper with additional neutron guides mounted between and after the chopper disks. (d) Photograph of the chopper cabinet that is shielded with both lead and cadmium.

The chopper is located inside a dedicated lead chopper housing (custom-made design, Von Gahlen Nederland B.V., Zevenaar, The Netherlands) as the absorption of neutrons by the chopper disks produces gamma radiation that needs to be shielded. On the inside, the lead is covered by a sandwich of 1 mm cadmium and 1 mm aluminum sheets. This was done to minimize neutron background while preventing direct contact with the cadmium sheets. Two sliding doors in the front allow access to the chopper when needed. In order to decrease the time needed for sample alignment, the chopper can be moved in and out of the beam using a pneumatic control system.

2. Wavelength resolution and chopper transmission

The major benefit of double-disk choppers is that the relative wavelength resolution is wavelength independent and can be tuned by the inter-disk distance z_0 . Indeed, ignoring the negligible contributions due to the finite height of the neutron beam, the finite detector thickness, uncertainty in the distance between the center of the chopper and the detector L_{TOF} , and the data acquisition and processing to the resolution, the wavelength resolution of a double-disk chopper is given by¹⁶

$$\frac{\Delta\lambda}{\lambda} = \frac{\Delta t_{\text{TOF}}}{t_{\text{TOF}}} \approx 0.68 \frac{z_0}{L_{\text{TOF}}}. \quad (1)$$

Here, t_{TOF} is the wavelength-dependent flight time of the neutron from the center of the chopper to the detector. This equation is valid for $\lambda < \lambda_0 = (h/m)(\phi/z_0 2\pi f)$ with h being Planck's constant and m being the neutron's mass.

Then, the transmission of the chopper, given by

$$T_c = Nf\Delta t_{\text{TOF}} \approx 0.68Nf\left(\frac{m}{h}\right)z_0\lambda, \quad (2)$$

mainly depends on the chopper frequency f and the inter-disk distance z_0 . In practice, f is chosen such that the neutrons within the wavelength range of interest $\lambda_{\text{min}} < \lambda < \lambda_{\text{max}}$ will arrive at the detector within the duty time $1/Nf$, i.e., $f \leq \frac{h}{m} \frac{1}{NL_{\text{TOF}}\Delta\lambda}$, with $\Delta\lambda = \lambda_{\text{max}} - \lambda_{\text{min}}$.

Figure 3 shows examples of spectra measured with different inter-disk distances z_0 . As can be seen, the intensity is proportional to z_0 . The relaxed resolution by increasing z_0 is visible at the Bragg structures in the spectrum around 0.45 nm.

B. Neutron optics

The ROG neutron reflectometer is connected to beam port R2m with a 19.4 m guide (NG1 in Fig. 4). It consists of fifteen 1292.33 mm sections of $40 \times 22 \text{ mm}^2$ $m = 2$ guides; each of these is fabricated by gluing three sections of 430.778 mm guide together using cold adhesive glue (Swiss Neutronics, Klingnau, Switzerland). Guide sections 1 and 14 have a vacuum connection that allows the guides to be evacuated using an ACP 28-40 dry multi-stage roots pump and has a base pressure $P = 10^{-1}$ mbar (Pfeifer Vacuum, Aßlar, Germany). It is supported by a frame made from Item Aluminum profiles (Item Systems B.V., Delft, The Netherlands) and shielded with 20 mm lead (Von Gahlen Nederland B.V., Zevenaar, The Netherlands).

Five evacuated neutron guides that are schematically indicated in Fig. 4 are positioned on the ROG neutron reflectometer to efficiently transport the neutrons from the chopper to the detector. The pre-sample and post-sample widths are 40 and 100 mm, respectively. The guides, with $m = 2$ coated sides and 0.5 mm-thick aluminum windows (Swiss Neutronics, Klingnau, Switzerland), are continuously evacuated with a base pressure of $P = 10^{-1}$ mbar (HiScroll 6, Pfeifer Vacuum, Aßlar, Germany).

1. Supermirrors

Two supermirrors can be used to deflect the neutron beam downward to facilitate the measurement of liquid samples. The first supermirror (indicated as SuMi0) is situated on a separate table, and the second (SuMi1) is situated on the frame. The use of these is discussed in Ch 4. The top surface of the supermirror has an $m = 4$ coating, allowing for a maximum glancing angle of $\theta_{\text{SuMi}} = \gamma\lambda$, with $\gamma = 70 \text{ mrad nm}^{-1}$. This results in a maximum glancing angle on a liquid sample $\theta = 4\theta_{\text{SuMi}}$. A maximum frame angle of $\theta = 80 \text{ mrad}$ allows for a minimum wavelength of 0.29 nm and a maximum wave-vector transfer of $Q = 3.5 \text{ nm}^{-1}$.

2. Frame overlap mirror

The purpose of the frame overlap mirror (indicated as FoMi) is to ensure that slow neutrons, i.e., those with a long wavelength, from the current pulse do not contaminate a subsequent pulse. As such, frame overlap is prevented by ensuring that neutrons with $\lambda > \lambda_{\text{cutoff}}$ do not reach the detector but are reflected out of the beam. The frame overlap mirror consists of a 0.5 mm-thick Si wafer with $m = 2$ coating on both sides, and the maximum wavelength λ_{cutoff} can be chosen by the glancing angle of the mirror, as shown in Fig. 5. The measured cutoff wavelength λ_{cutoff} is consistent with the $m = 2$ coating. The measured attenuation of the neutron beam through the frame-overlap mirror is 5%–15%, depending on glancing angle and wavelength (see Fig. 5).

3. Additional guides between the chopper disks

Between the chopper disks, additional $22 \times 40 \text{ mm}^2$ neutron guide sections with $m = 2$ coating on the sides can be positioned to increase the intensity at the sample position (SwissNeutronics AG, Klingnau, Switzerland). These sections have lengths of 250, 460, and

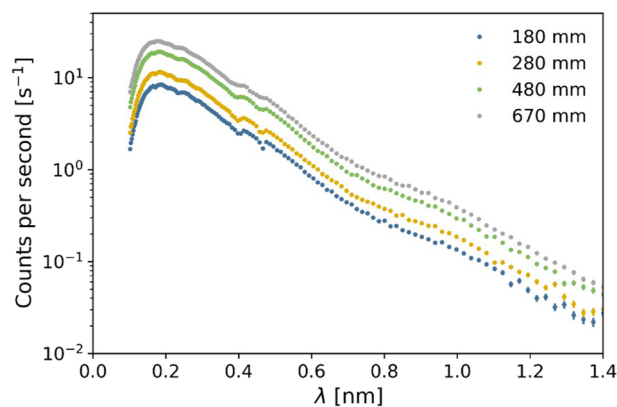


FIG. 3. Time-of-flight spectra measured with different inter-disk distances.

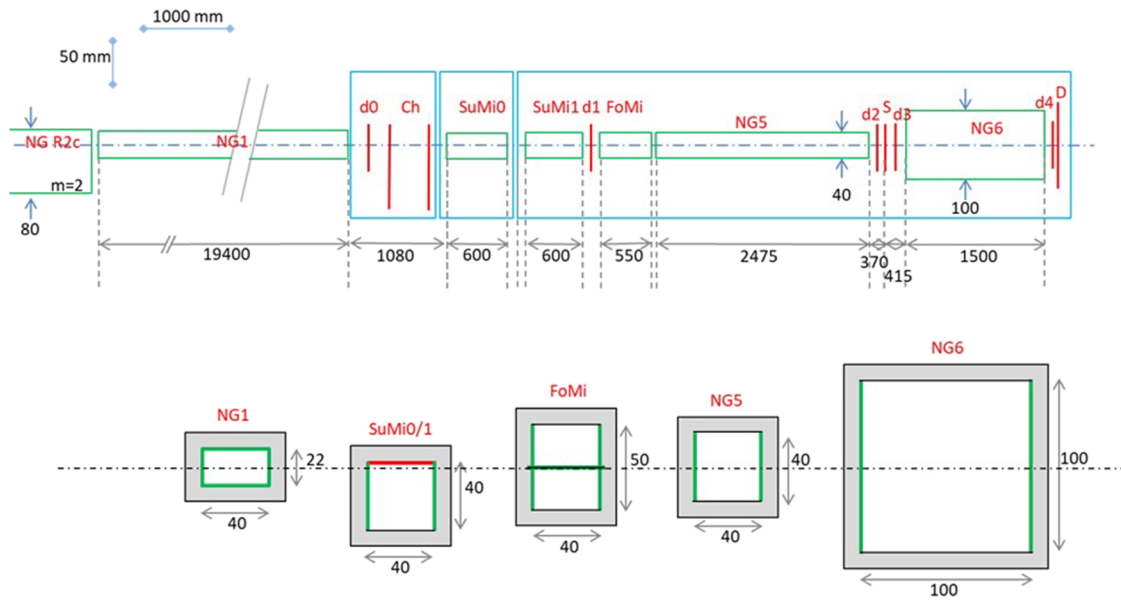


FIG. 4. Schematics of the neutron optics and their dimensions. The neutron guide (NG) sections are numbered from left (source) to right (detector). Top: side view; bottom: cross-sectional view where green indicates an $m = 2$ coating and red indicates an $m = 4$ coating.

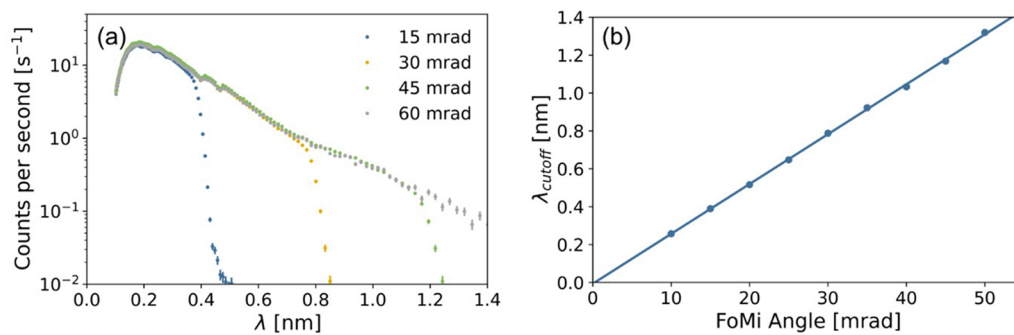


FIG. 5. (a) Wavelength spectrum transmitted by the frame overlap mirror as a function of its glancing angle. (b) Cutoff wavelength as a function of the glancing angle of the FoMi (FoMi angle).

650 mm, and the different lengths are to be used with different chopper settings. These guide sections are supported by a tailor-made holder (Fig. 2). Mounting blocks on the rear of the chopper cabinet ensure that the sections are always placed at exactly the same height and allow exchange within a few minutes. Indeed, only four bolts need to be tightened/untightened per guide section.

4. Intensity gain

Figure 6 shows the computed gain of the 40 mm wide neutron guides ($m = 2$) on the reflectometer with respect to the situation in which no neutron guides are used after the exit of NG1 that ends just before the chopper. In the calculations, we position a neutron guide after the chopper, i.e., at a distance of 1.08 m from NG1, and assume that there are no gaps between the guide sections and

no losses due to the windows of the guides. Details of the calculations are given in the supplementary material. As can be seen in Fig. 6, 20%–90% of neutrons are lost due to the wavelength dependent beam divergence if no guides are used. This loss is dramatically reduced by the positioning of the guides, leading to a gain of a factor of 1–5 depending on wavelength.

The insertion of the neutron guides between the chopper disks results in an extra increase in intensity. This is illustrated for the case with $z_0 = 280$ mm and placing extra neutron guides between (250 mm) and after (460 mm) the chopper disks. In the calculations, this is modeled by decreasing the gap between the entrance of the ROG and NG1 on ROG from 1.08 to 0.47 m. As can be seen, the experimentally determined gain ranges from about 10% at short wavelengths of $\lambda \approx 0.1$ nm to 30% at longer wavelengths of $\lambda > 0.8$ nm.

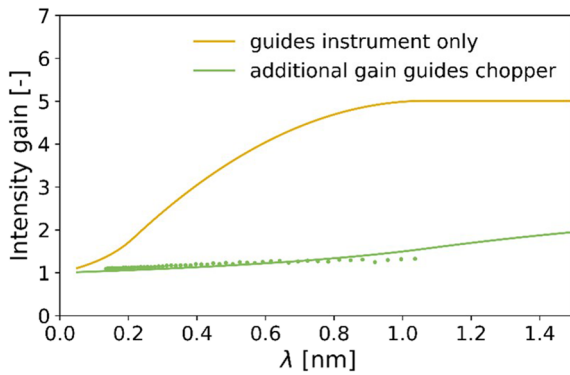


FIG. 6. Calculated intensity gain of the guides along the instrument (yellow) and additional gain of guides in the chopper (green). In the latter case, the intensity gain has also been measured as indicated by the points.

C. Diaphragms to control resolution and footprint

Two diaphragms, Dia 1 and Dia 2, before the sample are used to control the angular resolution and the footprint on the sample. These diaphragms are made from four 3 mm-thick boron nitride lamellae (in-house design and manufacturing) and separated by at least $l_{1-2} = 3128$ mm and are powered by two motors. The distance from Dia 1 to the sample is 3462 mm, and from Dia 2 to the sample variable is between 314 and 94 mm.

The angular resolution of the beam determines the resolution together with the wavelength resolution as set by selecting the distance between the chopper disks. In general, the resolution of a time-of-flight reflectometer is given by

$$\left(\frac{\Delta Q}{Q}\right)^2 = \left(\frac{\Delta \lambda}{\lambda}\right)^2 + \left(\frac{\Delta \theta}{\theta}\right)^2, \quad (3)$$

where the wavelength resolution is selected by the inter-disk distance of the chopper (see Sec. III A 1) and the angular resolution is given by¹⁶

$$\Delta \theta^2 = 0.68^2 \left(\frac{d_1^2 + d_2^2}{l_{1-2}^2} \right), \quad (4)$$

where d_1 and d_2 are the vertical openings of diaphragms 1 and 2, respectively, and l_{1-2} is the distance between the diaphragms. Assuming that the footprint of the neutron beam is completely within the sample, the intensity is given by

$$I \propto \frac{T_C d_1 d_2}{2l_{1-2}}, \quad (5)$$

with T_C being the transmission of the chopper (see Sec. III A 1).

In general, it is desirable to use $d_1 = d_2$ to obtain a certain resolution as this results in the highest intensity for a given resolution. However, in the case of finite samples, this may result in over illumination of the sample and thereby effectively a lower (reflected) intensity and effectively a higher resolution as the sample functions as a slit/diaphragm. Indeed, as the sample only reflects part of the beam, it reduces the divergence. Moreover, to obtain absolute reflection data by dividing the reflected intensities by the direct-beam intensities, the sample should not be over illuminated. This is especially important if no total reflection region is available for the sample of interest. In such a case, d_1 and d_2 are analytically optimized numerically to maximize the intensity for a given resolution while the footprint of the sample remains within the samples. Details of the calculations are given in the supplementary material. In this case, the intensity can be increased by shortening the distance from Dia 2 to the sample. An example is given in Fig. 7 and Table II. Here, we assume a total relative Q -resolution of 4%. Since both wavelength and divergence contributions in Eq. (3) are independent, the maximum intensity is obtained with equal contributions of 2.8%. In the calculations, the sample glancing angle is 8.5 mrad. For a different glancing angle, the diaphragm values can be scaled linearly,

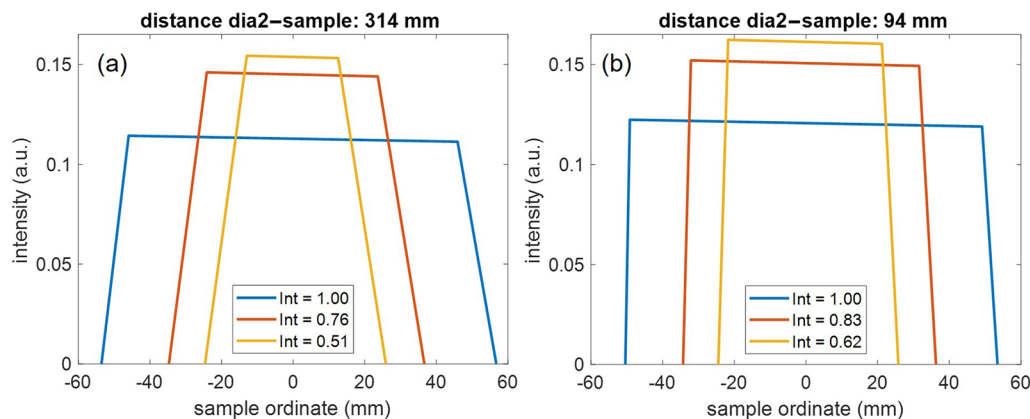


FIG. 7. Sample footprint for optimized intensity for an angular resolution $\Delta \theta / \theta = 2.8\%$ and a glancing angle $\theta = 8.5$ mrad for different sample sizes and two values for Dia 2-sample distances. Details are given in Table II. The sample ordinate is in the direction of the beam. The intensity values in the figure legend provide the intensity relative to the most optimal settings selected for an infinite sample with the same resolution.

TABLE II. Diaphragm settings for optimized intensity, given a relative angular resolution of 2.8% and a glancing angle of 8.5 mrad, as a function of sample size, for two different distances from the second diaphragm to center of the sample and a distance of $l_{1-s} = 3.462$ m between the first diaphragm to the center of the sample. The last column, Gain, shows for the specific samples sizes the gain that can be obtained by moving the slit closer.

Sample size (mm)	l_{1-2} (m)	l_{2-s} (m)	d_1 (mm)	d_2 (mm)	$I = d_1 d_2 / 2l_{1-2}$	Gain
>110	3.148	0.314	0.78	0.78	0.097	1.07
	3.368	0.094	0.84	0.84	0.104	
70	3.148	0.314	1.00	0.46	0.073	1.18
	3.368	0.094	1.04	0.56	0.086	
50	3.148	0.314	1.07	0.29	0.050	1.28
	3.368	0.094	1.12	0.39	0.064	

resulting in the same beam footprint on the sample. For a sample larger than ~ 100 mm, the maximum intensity can be reached for equal settings of both diaphragms. For smaller samples, the intensity is optimized. Decreasing the sample size will obviously lead to smaller intensities. The gain that can be obtained by bringing the second diaphragm close to the sample is more pronounced for smaller samples.

D. Sample compartment

The ROG has a closed sample compartment with dimensions of $760 \times 920 \times 1320$ mm³ (Fig. 8). Approximately in the center of the

compartment, a sample table that consists of a Huber 250×250 mm² 5203.30-X1 goniometer and a 5103.C20-X1 translation sample table equipped with VEXTA PK266-02B stepper motors, GEAR 2056.20 gearboxes, and HEIDNHAIN ROQ 425 absolute encodes (Huber Diffractionstechnik GmbH & Co. KG, Rimsting, Germany) is mounted. This table can achieve a maximum vertical displacement of 10 mm, ± 75 mrad in angle in the scattering plane, and ± 75 mrad in the direction orthogonal to the beam that is computer controlled. On top of the sample table, an anti-vibration table (similar to AVI-350M, The Table Stable Ltd., Mettmenstetten, Switzerland) can be mounted to minimize the influence of vibrations, which is especially important for measurements of liquid-liquid and liquid-air interfaces. Samples measured in air are typically positioned on top of a Thorlabs L490 178 \times 102 mm² lab jack with 57.5 mm manual vertical displacement and 34 kg load capacity (Thorlabs, Inc., Newton, New Jersey, United States), to which cadmium strips with a thickness of 1.0 mm are mounted to ease alignment and minimize background.

An additional diaphragm, Dia 3, is positioned just behind the sample table under normal operation to minimize background (IB-C120-AIR, JJ X-ray Hoersholm, Denmark). All 4 3×3 mm B₄C lamellae can be controlled independently of each other using Oriental Motors PK245M-01B stepper motors and Renishaw RL26BAE050D05F absolute encoders to achieve a diaphragm/slit opening range from full overlap of the blades to a maximum opening of 120×120 mm² with a 0.001 mm resolution.

E. Detector table and PRISM mount

Behind the sample compartment, a 2186×660 mm² detector table is positioned (Fig. 9), of which the angle can be varied

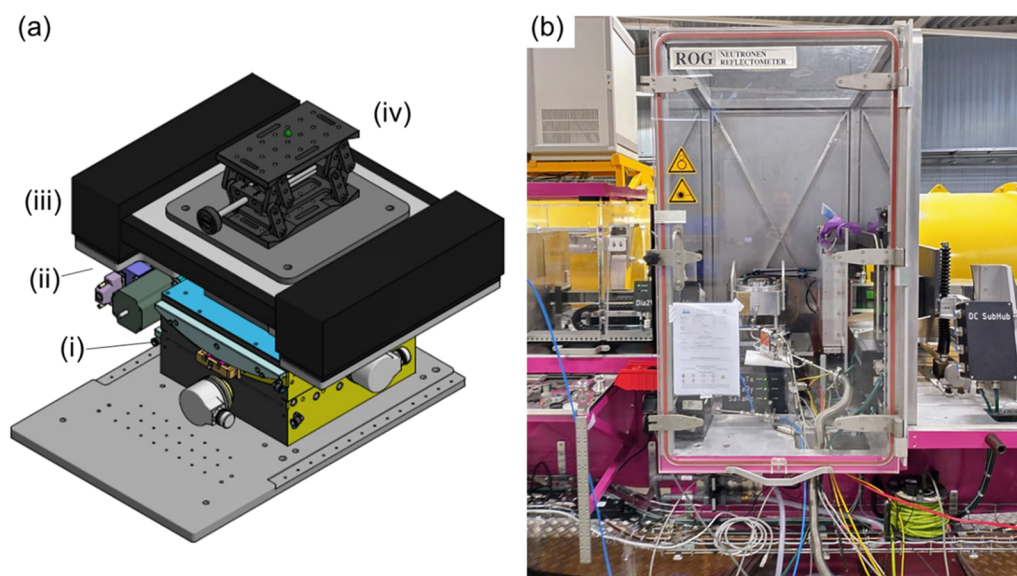


FIG. 8. (a) Schematics of the sample stage. The sample stage consists of (i) a computer controlled translation sample table to adjust the vertical displacement and a goniometer that allows one to adjust the angle parallel and orthogonal to the neutron beam. On top of the sample stage, (ii) an adapter plate is positioned to allow the mounting of the (iii) anti-vibration table. On top of the anti-vibration table, (iv) a Thorlabs lab jack is positioned for the measurement of samples in air. The green dot indicates the center of rotation and the center of the neutron beam. (b) Photograph of the sample space with a pressure and temperature controlled cell mounted.

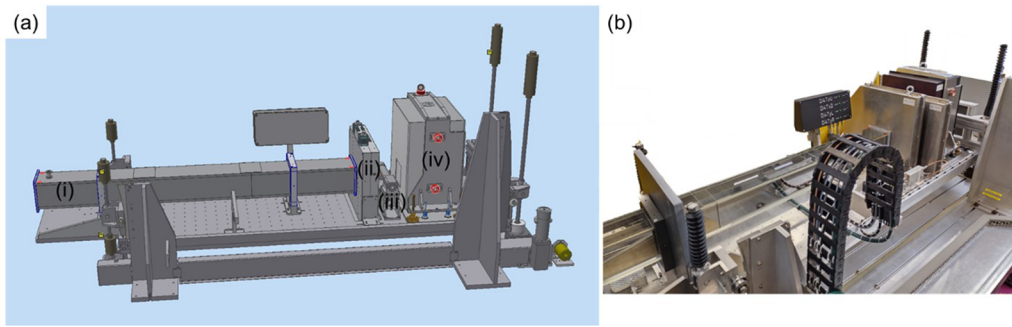


FIG. 9. (a) Schematics of the detector table. (b) Photograph of the detector table. Diaphragm 4 and the ^3He detector are inside two aluminum covers that are covered with cadmium from the inside. (i) $100 \times 100 \times 1500 \text{ mm}^3$ neutron guide with $m = 2$ side coating, (ii) diaphragm 4, (iii) ^3He detector that can be moved upright by pneumatic control out of the beam, and (iv) position sensitive detector.

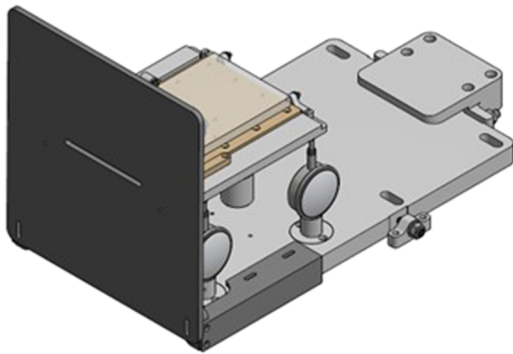


FIG. 10. Schematic of the addition to the detector table to accommodate a neutron prism for RAINBOWS measurements. The neutron prism, a $170.5 \times 100.5 \times 9.87 \text{ mm}^3$ MgF_2 single crystal (001 orientation) with a tangential concave radius of 94 m, is mounted on top of a table supported by four measurement clocks (0–10 mm with 0.01 mm resolution and a diameter of 53 mm, Ozaki MFG. Co., Ltd., Tokyo, Japan) to accurately set its height and angle. The single crystal is positioned on top of a polyether ether ketone (PEEK) support and kept in place using continuously pumping vacuum from below. A boron plastic screen with an opening of $80 \times 0.6 \text{ mm}^2$ is used as shielding and positioned in front of the prism.

between $-45 \text{ mrad} < \text{DtecRy} < 145 \text{ mrad}$. The point-of-rotation is exactly in the center of the neutron beam above the heart of the sample table. On the detector table, a $100 \times 100 \times 1500 \text{ mm}^3$ neutron guide with $m = 2$ side coating is positioned with 0.5 mm aluminum windows (SwissNeutronics AG, Klingnau, Switzerland). Behind the guide, the detector diaphragm Dia 4 is mounted to control the opening of the detector. This diaphragm has the same specifications as Dia 3.

To facilitate the RAINBOWS option, an additional component can be mounted on the detector table in front of the neutron guide (Fig. 10). This component includes a $170.5 \times 100.5 \times 9.87 \text{ mm}^3$ MgF_2 single crystal (001 orientation) neutron prism with a tangential concave radius of 94 m (Raw material: Korth Kristalle GmbH, Altenholz, Germany, and shaping and polishing: Winlight System, Saint Martin, France). To facilitate an accurate alignment of both the prism's height and angle with respect to the beam, the prism is mounted on

top of a table supported by four measurement clocks (0–10 mm with 0.01 mm resolution and a diameter of 53 mm, Ozaki MFG. Co., Ltd., Tokyo, Japan). Continuous vacuum pumping from below the table ensures that the prism keeps its position. Before the prism, boron plastic with an opening of $80 \times 0.6 \text{ mm}^2$ is used as additional shielding instead of Dia 3, while a cadmium sheet with an opening of $95 \times 1.0 \text{ mm}^2$ can be mounted in front of the neutron guide. (Dia 3 has to be removed to ensure enough space for the RAINBOWS add-on.)

F. Detectors

The ROG features two detectors, a XERAM 30NH1.5 ^3He detector that can be removed out of the beam by computer control and a $\text{ZnS:Ag}/^6\text{LiF}$ wavelength shifting fiber thermal neutron position sensitive detector that is described in Ref. 17. In short, the 1D PSD consists of 200 fibers with a diameter of 0.5 mm each. The data-acquisition electronics provides 521 pixels. Using a center of gravity interpolation algorithm, a position resolution, defined as the full width half maximum, of 0.3 mm is obtained. Both detectors are mounted in an aluminum enclosure that is covered with 1 mm cadmium to minimize the background. Behind the two detectors, a 40 mm Pb and a 5 mm B_4C beam stop is mounted.

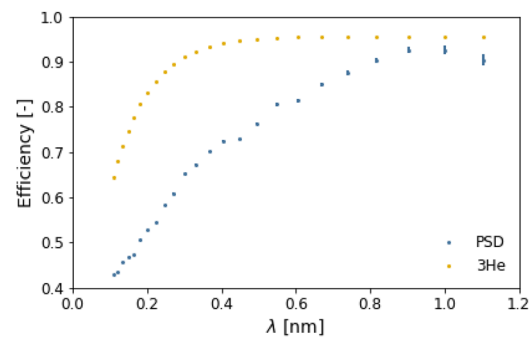


FIG. 11. Efficiency of the ^3He detector following Ref. 8 and the PSD detector.

The performance of the detectors is compared in Fig. 11, which shows the spectrum of the direct beam measured under exactly the same conditions. The ^3He detector has an efficiency that increases from $\varepsilon = 0.65$ at $\lambda = 0.1$ nm to $\varepsilon = 0.95$ at $\lambda = 1$ nm. As can be seen, the PSD has a slightly lower efficiency of about $\varepsilon = 0.42$ and $\varepsilon = 0.9$ at $\lambda = 0.1$ and $\lambda = 1.0$ nm, respectively. To improve the efficiency of the PSD at shorter wavelengths, a thicker scintillator can be used at the cost of a lower position resolution. However, a too thick scintillator can reduce the efficiency for longer wavelengths owing to the self-absorption of the generated photon in the scintillator material.

G. Shutter control

At the start of the neutron guide in front of the chopper, the neutron beam can be stopped by means of a compressed air operated shutter. This shutter can be opened (and closed) from a console next to the instrument control computer on the ROG-desk.

The shutter will automatically close (and cannot be opened):

1. when the door to the sample compartment of the ROG neutron reflectometer is opened,
2. when switched off by the computer,
3. when the pressure in the neutron guide exceeds 1 mbar,
4. when the air pressure drops below 2 bars (a buffer volume is incorporated in the supply line to ensure sufficient air capacity to close the shutter in case of failing air pressure), and
5. in the absence of AC-power.

The shutter status is monitored with signal lights (green = no beam, orange = shutter moving or position unclear, and red = beam open). Moving the shutter will also be signaled by a loud beep.

IV. MODES OF OPERATION

As illustrated in Figs. 1 and 12, the ROG neutron reflectometer can be used in three modes: mode (i) for solid samples, and mode (ii) and (iii) for liquid samples. The main difference between mode (i) and modes (ii) and (iii) is that in mode (i), the incoming beam is horizontal and the sample is tilted, whereas in modes (ii) and (iii), the incoming beam is bent downward to ensure the sample can remain horizontal.

To deflect the beam downward, one [mode (ii)] or two [mode (iii)] supermirrors can be used. The first supermirror, SuMi0, is located on a separate table, and its height is fixed. The second supermirror, SuMi1, is positioned on the frame that supports the remainder of the components. The position of this frame is controlled by 2 bars of variable length (Leg1 and Leg2), each connected by two pivot points. A 3001 mm-long stabilizer bar is connected to the top pivot point of Leg1 (see Fig. 9). The neutron beam has a fixed distance of 150 mm to the top surface of the pre-sample part of the frame and the top surface of the detector table.

In practice, mode (ii) is used for glancing angle on the sample of $\theta \leq 40$ mrad and only uses SuMi1, whereas in mode (iii), both supermirrors are used. Calculating the parameters (leg height, SuMi angles) for these two modes and a given sample glancing angle is

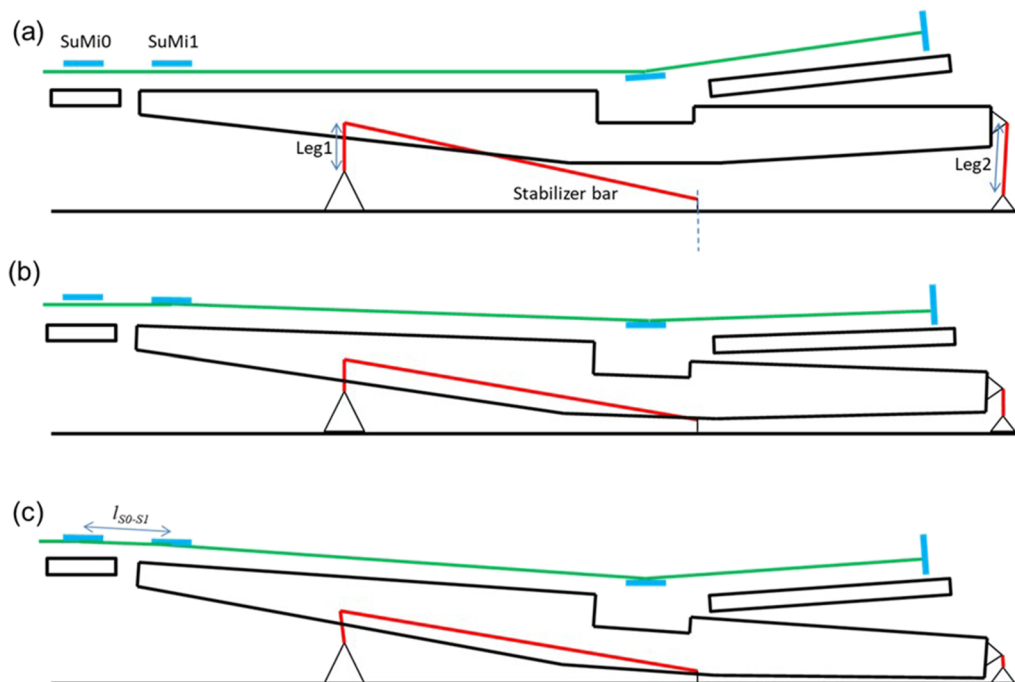


FIG. 12. Schematic configuration of different operation modes: (a) mode (i): solid samples with the incoming beam straight and the sample tilted. (b) mode (ii): liquid samples with $\theta \leq 40$ mrad. In this configuration, only SuMi1 deflects the incoming beam downward and the sample is positioned horizontally. (c) Mode (iii): liquid samples with $\theta > 40$ mrad. In this configuration, both SuMi0 and SuMi1 deflect the incoming beam downward and the sample is positioned horizontally.

quite tedious, and its details are given in the supplementary material. A few results are summarized in Table I. Note that for deflecting the beam downward, SuMi0 should be rotated clockwise, and SuMi1 that sits on the frame is counterclockwise. We also wish to note that by changing the length of Leg1 and/or Leg2, the distance between both supermirrors l_{S0-S1} , and consequently, the total flight path from the chopper to the detector will change.

The start of the flight path is the center of the double-disk chopper and thus depends on the inter-disk distance z_0 . Furthermore, it depends on the positioning of the frame, as shown in Table III, and the choice of detector,

$$L_{TOF} = l_{Ch-S0} - \frac{z_0}{2} + l_{S0-S1} + l_{S1-S} + l_{S-D},$$

with $l_{Ch-S0} = 1137$ mm being the distance from the first chopper disk to the center of the first supermirror, l_{S0-S1} being the distance between the two supermirrors, depending on the frame settings (see Table III), $l_{S1-S} = 3781$ mm being the distance from the second supermirror and the sample, and l_{S-D} being the distance between the sample and detector, which is 2065 and 2140 mm for the ^3He detector and PSD, respectively.

V. EXAMPLE OF A MEASUREMENT: HYDROGEN SENSING MATERIALS

We have performed measurements on a 40 nm $\text{HfH}_{1.6}$ thin film capped by a 10 nm Pd layer. This sample is the same as the sample used in Ref. 18. and was deposited using magnetron sputtering on a 3 in. fused quartz substrate (Esco Optics, Oak Ridge, New Jersey, United States of America) with a thickness of 5 mm, a roughness of <0.5 nm, and a flatness of 2 lambdas over 85% central. Detailed information about the sample preparation can be found in Refs. 19, and 20.

The measurements were performed with the double-disk chopper operating at $f = 17.7$ Hz and an inter-disk distance of $z_0 = 280$ mm and the ^3He detector. This results in a wavelength resolution of $\Delta\lambda/\lambda = 2.5\%$. The incident angle was set to $\theta = 8.5$ and 20 mrad. $d_1 = 1.2$ and $d_2 = 0.6$ mm were the sizes of diaphragms 1 and

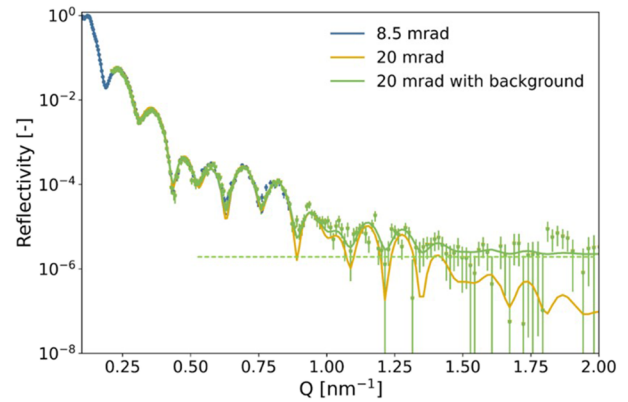


FIG. 13. Neutron reflectometry measurement on a 40 nm $\text{HfH}_{1.6}$ thin film capped by a 10 nm Pd layer. The measurement (dots) was performed at an incident angle of $\theta = 8.5$ and 20 mrad and for 6 and 18 h with a thermal spectrum, respectively. The continuous line indicates a fit to the data, of which one includes a background term evaluated to be 2×10^{-6} .

2, respectively, for the 8.5 mrad measurement, and the diaphragm was positioned 314 mm from the center of the sample. This results in a footprint of $64/88 \times 40$ mm² (umbra/penumbra) and a resolution of $\Delta Q/Q = 4.4\%$. For 20 mrad, the opening of the diaphragms was scaled to $d_1 = 2.8$ and $d_2 = 1.4$ mm to achieve the same footprint and resolution. The data were fitted using GenX3.^{21,22}

Figure 13 presents the measurements of the hafnium-based thin film. As can be seen, the measurements show a clear fringe pattern and have a good overlap. The reflectogram can be well described by a model in which the fitted parameters are within 0.5% of earlier published measurements performed at Offspec, ISIS Neutron Source, United Kingdom.¹⁸ Fitting the background provides a background of 2×10^{-6} in terms of reflectivity, which likely originates for the larger part from the sample itself. In addition, given the relatively low intensity of the present-day thermal neutron spectrum, this is low enough for practical purposes as measurements of reflectivity

TABLE III. ROG settings for the different modes of operation.

Mode	Glancing angle sample (mrad)	Glancing angle SuMi0 (mrad)	Glancing angle SuMi1 (mrad)	Leg1 (mm)	Leg2 (mm)	l_{S0-S1} (mm)
(i)	All	368.2	729.6	612.5
	10	...	5	354.4	661.2	613.5
	20	...	10	340.8	592.8	614.7
(ii)	30	...	15	327.2	524.5	616.1
	40	...	20	313.7	456.1	617.7
	40	10	10	327.0	469.7	620.6
(iii)	50	12.5	12.5	316.9	404.9	623.1
	60	15	15	306.0	340.1	625.9
	70	17.5	17.5	297.1	275.5	628.9
	80	20	20	287.4	210.9	632.1

below $\approx 10^{-5}$ are too time-consuming until the cold source has been installed. Recently, the upgraded ROG neutron reflectometer has also been used to study other hydrogen sensing materials^{23,24} *in situ* under hydrogen exposure using a tailor-made pressure and temperature controlled cell,²⁵ materials for nuclear waste storage,²⁶ and spin flippers.²⁷

VI. CONCLUSION

In conclusion, we have successfully renewed, relocated, and upgraded the ROG neutron reflectometer at the Delft Research Reactor. Innovations in the redesign include (i) a completely flexible redesigned double-disk chopper system allowing us to choose the optimal wavelength resolution with exchangeable neutron guides between the chopper disks to increase intensity, (ii) a movable second diaphragm just before the sample position to better control the sample footprint and effectively decrease counting times, (iii) the installations of neutron guides along the entire flight path, and (iv) the option to install a prism for wavelength discrimination using the wavelength-dependent refractive index of neutrons (RAINBOWS), of which the results will be discussed in an upcoming manuscript. Together, these innovations ensure an efficient use of neutrons to allow for an optimal performance of the reflectometer that can be further enhanced when a cold source is installed at the Delft Research Reactor.

SUPPLEMENTARY MATERIAL

The supplementary material contains (i) a description of the frame settings of the ROG, (ii) the calculations of the intensity loss due to the gap between neutron guides, (iii) a description of the various ROG settings, footprint, and resolution.

ACKNOWLEDGMENTS

The authors acknowledge the funding from the OYSTER (Optimised Yield – for Science, Technology and Education – of Radiation) program, funded by The Netherlands Organisation for Scientific Research (NWO). We thank Jeroen Plomp and Ernst van der Wal for fruitful discussions.

AUTHOR DECLARATIONS

Conflict of Interest

The authors have no conflicts to disclose.

Author Contributions

Lars J. Bannenberg: Conceptualization (equal); Data curation (equal); Formal analysis (equal); Investigation (equal); Methodology (equal); Project administration (equal); Resources (equal); Supervision (equal); Validation (equal); Visualization (equal); Writing – original draft (equal); Writing – review & editing (equal).
Raymon Bresser: Conceptualization (equal); Investigation (equal).
Piet van der Ende: Conceptualization (equal); Investigation (equal).
Martin van Exter: Conceptualization (equal); Investigation (equal).
William van Goozen: Investigation (equal). **Fred Naastepad:**

Software (equal). **Michel A. Thijs:** Conceptualization (equal); Investigation (equal). **Malte N. Verleg:** Conceptualization (equal); Investigation (equal); Visualization (equal). **Kees F. de Vroeghe:** Conceptualization (equal); Software (equal). **Rien Waaijer:** Investigation (equal). **Ad A. van Well:** Conceptualization (equal); Formal analysis (equal); Investigation (equal); Methodology (equal); Project administration (equal); Resources (equal); Supervision (equal); Validation (equal); Writing – original draft (equal); Writing – review & editing (equal).

DATA AVAILABILITY

The data that support the findings of this study are available from the corresponding author upon reasonable request.

REFERENCES

- J. Penfold, R. C. Ward, and W. G. Williams, “A time-of-flight neutron reflectometer for surface and interfacial studies,” *J. Phys. E: Sci. Instrum.* **20**(11), 1411 (1987).
- M. Gupta, T. Gutberlet, J. Stahn, P. Keller, and D. Clemens, “AMOR—The time-of-flight neutron reflectometer at SINQ/PSI,” *Pramana* **63**(1), 57–63 (2004).
- M. James, A. Nelson, S. A. Holt, T. Saerbeck, W. A. Hamilton, and F. Klose, “The multipurpose time-of-flight neutron reflectometer ‘Platypus’ at Australia’s OPAL reactor,” *Nucl. Instrum. Methods Phys. Res., Sect. A* **632**(1), 112–123 (2011).
- R. A. Campbell, H. P. Wacklin, I. Sutton, R. Cubitt, and G. Fragneto, “FIGARO: The new horizontal neutron reflectometer at the ILL,” *Eur. Phys. J. Plus* **126**(11), 107 (2011).
- J. Webster, S. Holt, and R. Dalglish, “INTER the chemical interfaces reflectometer on target station 2 at ISIS,” *Physica B* **385–386**, 1164–1166 (2006).
- V. Luter, H. Ambaye, R. Goyette, W. T. Hal Lee, and A. Parizzi, “Highlights from the magnetism reflectometer at the SNS,” *Physica B* **404**(17), 2543–2546 (2009).
- R. Cubitt and G. Fragneto, “D17: The new reflectometer at the ILL,” *Appl. Phys. A: Mater. Sci. Process.* **74**, 329–331 (2002).
- V. O. De Haan, J. De Blois, P. Van der Ende, H. Fredrikze, A. Van der Graaf, M. N. Schipper, A. A. van Well, and J. van der Zanden, “ROG, the neutron reflectometer at IRI, Delft,” *Nucl. Instrum. Methods Phys. Res., Sect. A* **362**(2–3), 434–453 (1995).
- R. Cubitt, J. Segura Ruiz, and W. Jark, “RAINBOWS: Refractive analysis of the incoming neutron beam over the white spectrum. A new fast neutron reflectometry technique exploiting a focusing prism,” *J. Appl. Crystallogr.* **51**(2), 257–263 (2018).
- W. Jark, “On the optimisation of the spectral resolution in spectrographs for cold neutrons based on refraction at grazing incidence,” *Nucl. Instrum. Methods Phys. Res., Sect. A* **735**, 291–296 (2014).
- R. Cubitt, H. M. Shimizu, K. Ikeda, and N. Torikai, “Refraction as a means of encoding wavelength for neutron reflectometry,” *Nucl. Instrum. Methods Phys. Res., Sect. A* **558**(2), 547–550 (2006).
- R. Cubitt and J. Stahn, “Neutron reflectometry by refractive encoding,” *Eur. Phys. J. Plus* **126**(11), 111 (2011).
- V. M. Pusekov, A. Schebetov, H. P. M. Gibcus, R. M. Gommers, F. Labohm, V. O. de Haan, and A. A. van Well, “Numerical calculation of neutron fluxes at the exit of a complex neutron-guide system at IRI, Delft,” *Nucl. Instrum. Methods Phys. Res., Sect. A* **492**(1–2), 105–116 (2002).
- V. O. de Haan, H. P. M. Gibcus, R. M. Gommers, F. Labohm, A. A. van Well, P. F. A. de Leege, A. Schebetov, and V. Pusekov, “A new method to determine *in situ* the transmission of a neutron-guide system at a reactor source,” *Nucl. Instrum. Methods Phys. Res., Sect. A* **484**, 451–458 (2002).
- A. A. Van Well, “Double-disk chopper for neutron time-of-flight experiments,” *Physica B* **180–181**, 959–961 (1992).
- A. A. Van Well and H. Fredrikze, “On the resolution and intensity of a time-of-flight neutron reflectometer,” *Physica B* **357**, 204–207 (2005).

- ¹⁷G. Mauri, G. J. Sykora, E. M. Schooneveld, and N. J. Rhodes, “Enhanced position resolution for ZnS:Ag/⁶LiF wavelength shifting fibre thermal neutron detectors,” *Eur. Phys. J. Plus* **136**(3), 286 (2021).
- ¹⁸C. Boelsma, L. J. Bannenberg, M. J. Van Setten, N. J. Steinke, A. A. Van Well, and B. Dam, “Hafnium—An optical hydrogen sensor spanning six orders in pressure,” *Nat. Commun.* **8**(1), 15718 (2017).
- ¹⁹L. J. Bannenberg, C. Boelsma, H. Schreuders, S. Francke, N. J. Steinke, A. A. Van Well, and B. Dam, “Optical hydrogen sensing beyond palladium: Hafnium and tantalum as effective sensing materials,” *Sens. Actuators, B* **283**, 538–548 (2019).
- ²⁰L. J. Bannenberg, H. Schreuders, H. Kim, K. Sakaki, S. Hayashi, K. Ikeda, T. Otomo, K. Asano, and B. Dam, “Suppression of the phase coexistence of the fcc–fct transition in hafnium-hydride thin films,” *J. Phys. Chem. Lett.* **12**(45), 10969–10974 (2021).
- ²¹A. Glavic and M. Björck, “GenX 3: The latest generation of an established tool,” *J. Appl. Crystallogr.* **55**(4), 1063 (2022).
- ²²M. Björck and G. Andersson, “GenX: An extensible X-ray reflectivity refinement program utilizing differential evolution,” *J. Appl. Crystallogr.* **40**(6), 1174–1178 (2007).
- ²³L. J. Bannenberg, H. Schreuders, N. van Beugen, C. Kinane, S. Hall, and B. Dam, “Tuning the properties of thin-film TaRu for hydrogen-sensing applications,” *ACS Appl. Mater. Interfaces* **15**, 8033 (2023).
- ²⁴L. J. Bannenberg, L. Blom, K. Sakaki, K. Asano, and H. Schreuders, “Completely elastic deformation of hydrogenated Ta thin films,” *ACS Mater. Lett.* **5**, 962–969 (2023).
- ²⁵L. J. Bannenberg, M. van Exter, M. N. Verleg, B. Boshuizen, S. R. Parnell, M. Thijs, and H. Schreuders, “Versatile pressure and temperature controlled cell for neutron reflectometry and small-angle neutron scattering,” *J. Neutron Res.* (published online) (2023).
- ²⁶A. Situm, B. Bahadormanesh, L. J. Bannenberg, F. Ooms, H. A. Feltham, G. Popov, M. Behazin, L. V. Goncharova, and J. J. Noël, “Hydrogen absorption into copper-coated titanium measured by in situ neutron reflectometry and electrochemical impedance spectroscopy,” *J. Electrochem. Soc.* **170**(4), 041503 (2023).
- ²⁷E. Babcock, Z. Salhi, A. Feoktystov, L. J. Bannenberg, S. R. Parnell, D. Alba Venero, V. Hutanu, H. Thoma, J. Xu, P. Pistel, J. Damean, A. Ioffe, and S. Mattauch, “In-situ ³He neutron spin filters at JCNS, status and updates,” *J. Phys.: Conf. Ser.* **2481**(1), 012009 (2023).